Nat Immunol. Author manuscript; available in PMC 2016 August 03.

Published in final edited form as:

Nat Immunol. 2013 August ; 14(8): 785–792. doi:10.1038/ni.2631.

Nucleation of platelets with bloodborne pathogens on Kupffer cell precedes other innate immunity and contributes to bacterial clearance

Connie H. Y. Wong[1,3,*], **Craig N. Jenne**[2,*], **Björn Petri**[1], **Navina L. Chrobok**[1,4], and **Paul Kubes**[1,2]

[1]Calvin, Phoebe & Joan Snyder Institute for Chronic Diseases, Department of Physiology and Pharmacology, University of Calgary, Alberta, Canada

[2]Calvin, Phoebe, & Joan Snyder Translational Laboratory in Critical Care Medicine, Department of Critical Care Medicine, University of Calgary, Alberta, Canada

Abstract

Using intravital imaging of the liver, we unveil a collaborative role for platelets with Kupffer cells (KCs) in eradicating bloodborne bacterial infections. Under basal conditions, platelets via glycoprotein Ib (GPIb) formed transient "touch-and-go" interactions with von Willebrand factor (vWF) constitutively expressed on KCs. Bacteria, such as *Bacillus cereus* and Methicillin-resistant *Staphylococcus aureus* (MRSA), were rapidly caught by KCs and triggered platelets to switch from "touch-and-go" to sustained GPIIb-mediated adhesion on the KC surface to encase the bacterium. Infected $GpIb\alpha^{-/-}$ mice demonstrated increased endothelial and KC damage, leading to increased fluid leakage, significant polycythemia and rapid mortality. This study identifies a novel surveillance mechanism of intravascular macrophage by platelets that rapidly converts to a critical host response against bloodborne bacteria.

Keywords

Immune surveillance; platelet aggregation; imaging

Correspondence should be addressed to: P.K. (pkubes@ucalgary.ca), Calvin, Phoebe & Joan Snyder Institute for Chronic Diseases, Department of Physiology and Pharmacology, University of Calgary, HRIC 4A26A, 3280 Hospital Drive N.W., Calgary, Alberta, Canada T2N 4N1, Telephone: +1 403 220 8558, Facsimile: +1 403 270 7516, pkubes@ucalgary.ca.

[3]Current affiliation: Department of Immunology (Clayton), Monash University, Australia.

[4]Current affiliation: Department of Anatomy and Neurosciences, Neuroscience Campus Amsterdam, VU University Medical Centre, Amsterdam, The Netherlands.

[*]These authors contributed equally.

AUTHOR CONTRIBUTIONS

C.H.Y.W. and C.N.J. designed and did the majority of the experiments and C.H.Y.W. prepared the manuscript; B.P. did all of the muscle, skin and ear experiments. N.L.C. contributed some liver imaging experiments; C.N.J did all of the revisions and additional experiments; and P.K. provided overall supervision, helped design all of the experiments and prepared the manuscript.

COMPETING FINANCIAL INTERESTS

The authors declare no competing financial interests.

INTRODUCTION

Innate immunity is the most ancient defense system for vertebrates against microbes. The host innate immune defense comprises of an array of cells with sensitive receptors that detect microbial products and instigate a counterattack upon infection. The gut is a likely entry portal for pathogens into the host and, as such, many immune cells reside within the liver, an organ that filters blood as it perculates through the vast array of vascular sinusoids. In fact, the liver is becoming increasingly known for its immunological roles, including its ability to eradicate the vasculature of systemic infections via an ongoing constitutive network of intravascular macrophages called Kupffer cells (KCs)[1]. KCs are strategically positioned and reside as stationary macrophages within the liver sinusoids to trap, phagocytose and remove pathogens in transit through the circulation. Indeed, efficient binding of blood-borne pathogens to the KC surface constitutes the first-line of host immune defence in the circulation[2, 3].

The survival of a pathogen is dependent on its ability to evade the well-evolved host immune response. No pathogens have been more successful in this regard than the human pathogens *Staphylococcus aureus* (*S. aureus*) and the spore-forming *Bacillus* family, which have found ways to survive the hostile intracellular environment of macrophages. *S. aureus* produces numerous toxins that cause cell lysis[4, 5], while the spores of *Bacillus* can germinate, multiply and escape from host cells[6–9]. *Bacillus anthracis* (*B. anthracis*) is highly virulent to mammals and is the causative agent of anthrax[10]. In addition, *Bacillus cereus* (*B. cereus*) isolates have been implicated in lethal infections with similar clinical presentation to *B. anthracis*, thus posing a potential serious public health problem[11, 12]. Despite the presence and accumulation of immune cells at the site of infection, these infections are characterized by bacteremia and severe tissue damage leading to death[13]. In fact, *B. cereus* contains many bacterial factors that induce phagocytic cell death[14, 15], and potentially cause major host tissue damage and compromise the antimicrobial immune response.

In addition to the professional phagocytes, there is growing interest in the role of platelets in immunity. Platelets express many major innate immune receptors, including most Toll-like receptors (TLRs), thrombin receptors, complement receptors and numerous adhesion molecules [16]. In fact, platelets are able to recognize molecular features of microbes and contain many important immunomodulating mediators essential for alerting and recruiting immune cells[17–19]. Indeed, the appropriate interplay between, for example, monocytes and platelets leads to increased production of various cytokines[20], and interactions between neutrophils and platelets leads to the production of neutrophil extracellular traps (NETs)[18, 21]. Platelets have also been shown to produce various anti-microbial molecules, including defensins[22], thrombocidins[23] and kinocidins[24], suggesting they are capable of interacting with and killing bacteria directly[25]. Despite this, how direct contact between platelets and bacteria might occur in the mainstream of blood, under shear conditions, is completely unclear. One possibility is that bacteria might inadvertently collide with platelets in the circulation. However, immune events are usually not left to chance. Therefore, rather than a haphazard approach for platelet-bacterial interactions, a systematic and purposeful approach must exist to allow platelets to interact with bacteria.

Intriguingly, recent work has shown that members of the *Bacillus* family can induce platelet aggregation within minutes following the exposure of *B. cereus* to human or mouse blood in an *in vitro* flow chamber assay[26]. These aggregates could either potentially shield the bacteria from immune cells, or be a mechanism to enlist the help of platelets to eradicate the bacteria. If the latter is true, then it is likely that platelets may patrol the vasculature in a systematic way and in some manner co-localize with blood-borne bacteria. We recently noted that platelets after 4 h of lipopolysaccharide (LPS) stimulation could bind neutrophils as well as Kupffer cells while the former was critical for NETs it was unclear why platelets would interact with Kupffer cells[27]. Herein, using the multi-channel intravital spinning-disk confocal microscope, we observed, independent of any stimulus, a novel patrolling mechanism of platelets in blood that involved ongoing "touch-and-go" Glycoprotein Ib (GPIb), also known as CD42, interactions with constitutively expressed vWF on KCs in liver sinusoids under basal conditions. We used *B. cereus* as a model pathogen (but also MRSA) and found that the surface of the KCs became the battleground where caught bacteria now encountered a swarm of platelets that converted their "touch-and-go" behavior to a sustained GPIIb/IIIa-dependent adhesion and actively encased the bacteria for eradication within the first minute of encounter. This previously undescribed mechanism preceded all other innate immune cell recruitment and was critical for host survival in response to gram-positive bacteria.

RESULTS

A novel platelet patrolling mechanism in liver

Intravital spinning-disk confocal microscopy of the liver microvasculature revealed a continuous "touch-and-go" (shorter than 1 sec) behavior of individual circulating platelets within the sinusoids of the liver (Fig. 1a). Addition of fluorescent tagged antibody against F4/80 revealed a vast network of KCs lining the lumenal side of sinusoids and under basal conditions a substantial number of circulating platelets transiently touched these immobilized KCs (Fig. 1b,c). Platelets could also be seen touching the sinusoidal endothelium (Fig. 1b). Very few platelets attached to the KCs for an extended period and even fewer aggregates were observed, suggesting little or no activation under basal conditions (Supplementary Video 1). Depletion of KCs with clodronate liposomes reduced the number of platelets that interacted with the liver sinusoids (Fig. 1c), with the few remaining interactions involving platelets touching down on the endothelium (Fig. 1b). We examined four other tissues and observed many fewer "touch-and-go" interactions in brain, muscle, skin and ear where there are no intravascular macrophage (Fig. 1d). The behavior of these "touch-and-go" interactions in the liver was reminiscent of catch bonds described for the platelet adhesion receptor GPIb. Indeed, we saw fewer of these platelet "touch-and-go" interactions in the liver of $GpIb\alpha^{-/-}$ mice, suggesting that interactions with KCs but not endothelium were entirely GPIb-dependent (Fig. 1c). Deficiency of another integrin on platelets, GPIIb, also known as CD41 or ITGA2B, did not affect the "touch-and-go" behavior on KCs or endothelium (Fig. 1b). These findings reveal a novel surveillance mechanism whereby platelets survey the surface of intravascular macrophages in the liver.

Platelets respond rapidly to *B. cereus in vivo*

Platelets are essential for primary hemostasis and are becoming increasingly recognized for their role in immunity and inflammation[17–19]. In control mice, the circulating blood platelet count was approximately 8.5×10^8/ml, this number was markedly reduced 4 h after infection with our model bacterium, *B. cereus* (Fig. 2a). Within the first 4 h of *B. cereus* infection, most wild-type mice survive with less than 10% mortality observed in this population (Fig. 2b). In contrast, all mice that were depleted of platelets prior to infection died within 4 h post-infection (Fig. 2b). Although the amount of *B. cereus* given was sufficient to cause absolute lethality in all platelet-depleted mice, some platelet-sufficient mice managed to survive indefinitely. These data indicate platelets play a fundamental and critical role in the rapid host defense and early survival against the lethal pathogenic bacterium, *B. cereus*. The majority of bacteria were trapped within the liver with an order of magnitude less in lungs and spleen (Fig. 2c). Key clearance mechanisms must occur early in response to this pathogen as within 1 h of infection, bacteremia was low and all bacteria were eliminated from blood by 4 h in platelet-sufficient mice (Fig. 2d). In contrast, bacteremia was increased in platelet-depleted mice at both 1 and to a lesser extent at 4 h post infection prior to death (Fig. 2d). Collectively, these data suggest that platelets play a role in host-defense to *B. cereus* and help facilitate clearance of this pathogen by the liver.

Platelets dock on KCs following *B. cereus* infection

Rapid trapping of *B. cereus* was mediated by KCs (within seconds) in the liver vasculature. Immediately following pathogen capture, time-lapsed videos demonstrated that the “touch-and-go” behavior of platelets was converted to a profound sustained recruitment of platelets to the KC surface (Fig. 3a; Supplementary Video 2) with subsequent encasement of the bacteria by the platelets. These platelet aggregates preferentially co-localized with KCs that had captured *B. cereus* (Fig. 3a, yellow arrows). On occasion, aggregates were also observed forming at a distance from any *B. cereus* (Fig. 3a, white arrowhead). Quantification of the size of the aggregates revealed a significant increase in the number of both small (10 μm^2) and large (25 and 50 μm^2) platelet aggregates within the livers of *B. cereus* infected mice (Fig. 3b). This behavior persisted throughout the observational period (30 min; Fig. 3c). Heat-killed *B. cereus* failed to induce platelet aggregation in the liver throughout the first 30 min observational period (Fig. 3c), suggesting that a metabolically active bacterium is necessary to induce such host immune response.

To better visualize and understand the progression from capture of *B. cereus* to platelet recruitment, we used high magnification and 4-D reconstruction (3-D reconstruction in real time). One such example shows a KC in blue with no *B. cereus* and no large platelet aggregates (Fig. 3d, top left panel - 0 min). Within the first minute, *B. cereus* binds to the KC (white arrow). Within seconds following bacterial capture, platelets begin to bind to the KC and within 1 min a substantial aggregate can be seen enveloping the *B. cereus* (Fig. 3d, top right panel) which over the next 3 minutes completely covers the *B. cereus* (Fig. 3d, bottom panels). Clearly, the 4-D imaging reveals that the platelets form an encasement around the trapped *B. cereus* on the surface of KCs.

Platelets dock on KCs following MRSA infection

The observation of platelet encasement of bacteria was not restricted to *B. cereus*. A strain of community-associated Methicillin-resistant *S. aureus* (MRSA; USA300) also induced platelet recruitment and aggregation on KCs post-infection (Fig. 4a). Surprisingly, the Methicillin-susceptible strain of *S. aureus* (MSSA; Xen29) failed to initiate platelet aggregation (Fig. 4a), suggesting this platelet surveillance system exists to deal with a specific subset of pathogens. In a similar manner to the *B. cereus*-infected mice, platelet aggregations in the liver preferentially co-localized with KCs that had captured MRSA (Fig. 4b, yellow arrows). In addition, mice depleted of platelets demonstrated greater mortality 8 h and 12 h post-MRSA infection (Fig. 4c), suggesting that the platelet docking and encasing of bacteria within the liver may contribute to rapid host defense and early survival against certain blood-borne pathogens. Moreover, the mechanisms behind this rapid nucleation of platelets post-infection appear to be largely independent of the TLR pathways that use MyD88 (Supplementary Fig. 1). All of these events preceded any neutrophil recruitment, which was entirely MyD88 dependent (Supplementary Fig. 2). Therefore, the platelet recruitment is likely neutrophil independent.

Platelet aggregation requires bacterial capture by KCs

We next investigated the mechanisms by which platelets rapidly accumulate on KCs after bacterial infection *in vivo*. To determine whether it is the KCs or the bacteria that cause the observed platelet firm adhesion on the vessel wall, we treated a group of mice with chlodronate liposomes (CLL) to deplete KCs. Complete KC depletion was achieved with CLL, whereas at least 40 KCs per microscopic field of view are seen in untreated mice (Fig. 5a). Treatment with CLL significantly reduced the number of *B. cereus* caught in liver sinusoids (Fig. 5b). Importantly, although all KCs were gone, a few *B. cereus* could be seen in the sinusoids binding directly to the vessel wall (Supplementary Video 3). This bacterial binding however was not sufficient to induce platelet aggregation as platelet aggregates were not observed in these KC-depleted mice (Fig. 5c), indicating KC capture of bacteria was essential for platelet recruitment and aggregation. Indeed, even the minor aggregation seen in sham-treated mice was eliminated in the absence of KCs (Fig. 5c). Complement opsonization is also necessary for the clearance of *B. cereus*. In fact, like KC-depleted animals, $C3^{-/-}$ mice demonstrated similar reductions in *B. cereus* capture (Fig. 5b) and platelet aggregation (Fig. 5d). Thus the interaction of *B. cereus* with both KC and complement is necessary for the induction of platelet aggregation.

GPIb, vWF and GPIIb recruit platelets to KCs

The platelet adhesion molecule GPIb has been reported to bind with vWF allowing for platelet adhesion and aggregation at sites of vascular injury[28]. $GpIb\alpha^{-/-}$ mice failed to accumulate platelets on KCs after *B. cereus* infection, suggesting this platelet receptor is critical in the bacterial-induced platelet recruitment (Fig. 6a). To determine how the GPIb on platelets bound to KCs, we stained for various proteins and surprisingly found high amounts of von Willebrand factor (vWF) deposition within liver sinusoids (Fig. 6b). What was more intriguing was the fact that in addition to vWF staining on endothelium (Fig. 6c, white arrowheads), there were large clusters of vWF on the KCs (Fig. 6c, yellow arrows).

Blockade of vWF significantly inhibited platelet accumulation after *B. cereus* capture by KCs (Fig. 6d). Although we had expected to see no vWF deposition under control conditions in the sinusoids, we observed substantial staining on KCs in the absence of any bacteria (Fig. 6c). In fact, although a significant increase of vWF staining was observed following *B. cereus* infection, it is important to note that considerable constitutive vWF expression exists within the liver vasculature (Fig. 6b). This basal expression of vWF potentially contributes to the GPIb-mediated platelet docking on KCs as part of the surveillance mechanism described in Fig. 1. Although, the vWF and GPIb are critical to dock platelets on the surface of KCs, this docking appeared transient and it was only after *B. cereus* was caught did the platelet "touch-and-go" interaction convert to sustained adhesion. It is well established that GPIb is thought to induce tethering, but not firm adhesion to vWF[29]. In fact, GPIb-dependent aggregation has only been reported at extremely high shear (>10,000 sec^{-1}) associated with stenotic arteries, and not in low shear environment of the liver sinusoids. However, GPIb is not the only receptor on platelets for vWF. In fact, it was previously demonstrated that vWF is able to mediate firm adhesion of platelets via a second platelet receptor, GPIIb/IIIa. To test this potential adherence mechanism, we infected mice deficient of GPIIb receptor (*Cd41-yfp*$^{ki/ki}$) with *B. cereus*. Indeed, we observed severely reduced platelet accumulation on the surface of KCs of *Cd41-yfp*$^{ki/ki}$ mice following infection (Fig. 6e), despite no affect on the initial "touch and go" surveillance (Fig. 1b,c). From these experiments we have determined that interactions between vWF and GPIb support the "touch and go" surveillance of KC by platelets whereas it is the interaction between vWF and GPIIb/IIIa that mediates the accumulation of platelets following capture of *B. cereus* by KC.

Platelet recruitment protects the host post-infection

There was less than 10% mortality in wild-type mice within the first 4 h of *B. cereus* infection (Fig. 7a). By contrast, more than 80% of mice deficient in GPIb (*GpIbα*$^{-/-}$) died within 4 h post infection (Fig. 7a). Similar to platelet-depleted mice, we observed profoundly elevated bacteremia in *GpIbα*$^{-/-}$ mice at 1 h post infection compared to their wild-type counterparts (Fig. 7b). Importantly, nearly identical results were also observed for MRSA (Fig. 4c). *GpIbα*$^{-/-}$ mice were also unable to reduce *B. cereus* numbers in blood 4 h post infection (Fig. 7b). The inability to control *B. cereus* infection was more pronounced in GPIb-deficient mice than in platelet-depleted mice (probably due to only a 90% reduction in circulating platelets following depletion), and highlights the critical importance of GPIb. Most septic infections do not originate in the bloodstream but rather from some other infectious focus and then enter the blood. To model this process, we utilized an intraperitoneal challenge with *B. cereus*. Again, the ability of platelets to shield the host from *B. cereus* was essential to host survival as mice deficient for platelets (or the important platelet receptor, GPIb) had reduced survival when compared to platelet-sufficient mice (Supplementary Fig. 3). Together, these data indicate that platelet accumulation and encasement of *S. aureus* and *B. cereus* is essential to the host defense against these pathogens.

The inability to efficiently respond to a *B. cereus* infection caused overt liver injury, dysfunction and cell death. Wild-type animals infected with *B. cereus* displayed some

hepatic damage assessed by elevated serum alanine aminotransferase (ALT) concentrations, however *GpIbα*$^{-/-}$ mice exhibited significantly greater elevations of serum ALT at 4 h after *B. cereus* (Fig. 7c). There was also a significantly greater frequency of PI-positive staining (cell death) in the infected livers of *GpIbα*$^{-/-}$ mice compared to their wild-type counterparts and this staining co-localized with both the endothelial lining of the liver sinusoids and with KCs (Fig. 7d). Quantification of this staining confirmed only minimal cell death in wild-type mice, but a very large (ten-fold) increase in PI-positive staining in the livers of *GpIbα*$^{-/-}$ post-infection (Fig. 7e). We also observed cellular dysfunction in both the endothelium and KCs. A significant increase in plasma leakage was observed as evidenced by a rise in hematocrit from 40% to 50% at 4 h after *B. cereus* infection (Fig. 7f). In the surviving *GpIbα*$^{-/-}$ mice, a three-fold greater increase in hematocrit values was noted post infection, reaching a value of nearly 70% within 4 h post-infection (Fig. 7f). The amount of hemoglobin was similar in the two strains of mice suggesting a loss of fluid rather than an increase in red blood cell number (data not shown). KCs of infected livers of *GpIbα*$^{-/-}$ mice but not wild-type mice had impaired trapping capacity. Catching of inert microspheres injected intravenously was the same under control conditions (Fig. 7g). However, following *B. cereus* infection, there was a significant reduction in the number of microspheres captured in the livers of *GpIbα*$^{-/-}$ mice (Fig. 7g). This finding potentially explains the increased circulating *B. cereus* seen at 4 h in *GpIbα*$^{-/-}$ mice. There was also some sign of exacerbated inflammation in other organs as we observed an exacerbated increase in neutrophil recruitment to the lungs of infected *GpIbα*$^{-/-}$ mice compared to their wild-type counterparts perhaps reflecting greater bacterial dissemination in the *GpIbα*$^{-/-}$ mice (Fig. 7h). Failure of platelets to encapsulated the bacterium and shield the host results increased cellular dysfunction and death in the liver leading to vascular damage and the inhibition pathogen capture by KCs. A diagram to illustrate the interactions between the different cell types and molecules is shown in Supplemental Figure 4.

DISCUSSION

Although platelets continue to be regarded as small cell fragments that only participate in hemostasis, their origin, membrane receptors and intracellular contents provide irrefutable support for the view that platelets play a central role in fighting infections. In invertebrates, the hemocyte participates both hemostasis and in the defense against pathogens, acting as an ancient granulocyte[30]. Indeed, the platelet has retained many features of the prototypical granulocyte, including the ability to respond to infections via archetypal pattern recognition receptors such as TLRs[18]; changing from discoid to ameboid shape in the presence of infections[31]; chemotaxing towards signature bacterial motifs such as formylated peptides[32]; and release of oxidants and potent anti-microbial proteins (defensins, etc)[33]. In this study, we find that the platelet actively patrols the vasculature, forming touch-and-go interactions with KCs in the liver sinusoids. These interactions convert rapidly to firm adhesion once specific microbes are caught by KCs. Although it had been shown that platelets can attach to, and kill microbes in the confines of a test tube under static conditions[34, 35], the mechanism by which platelets could possibly trap bacteria in the dynamic conditions of blood flow remained unknown. In this study, using dual-camera multi-channel spinning disk intravital confocal microscopy, we were able to unveil a previously unknown innate immune

mechanism. Platelets co-localize to sites of bacterial capture on KCs where they encapsulate and help facilitate the killing of the microbe.

Intravital imaging revealed that platelets transiently interact predominately with KCs but also with endothelium under basal conditions. Indeed, when KCs were depleted the number of patrolling platelets was greatly diminished. Moreover, tissues like brain, skin or muscle that lack KCs revealed few patrolling platelets. Catch bonds with their short on rates and fast off rates, formed by GPIb and vWF would predict the rapid “touch-and-go” baseline interactions we observed in the uninfected liver. KCs have previously been reported to clear blood of vWF[36], however our data suggest that this apparent clearance may actually be part of an essential innate immune surveillance mechanism, whereby vWF is concentrated on the KC surface creating “landing pads” for circulating platelets. These vWF hotspots on KC surface become reactive for platelets, allowing for rapid, transient docking, a hallmark feature of tethering via catch bonds. Although this type of vWF clearance has also been reported in spleen, patients who underwent splenectomy did not show the expected rise in vWF concentrations suggesting a dominate role for the liver in the sequestration of vWF[37]. Therefore, despite the relevance of spleen as an important immune organ, we speculate the vast majority of the patrolling interactions between platelets and intravascular macrophages occur in the liver. As such, it is the liver that represents the critical platform for platelet surveillance and protection from highly pathogenic, blood-borne infections.

We used *B. cereus* in this study, as it best highlighted the critical importance of platelets in mammalian immunity against pathogens, and suggested no redundancy for platelets in this system. Without platelet immunity, mammals would be far more susceptible to these infections. Our observations are not restricted to *B. cereus*, as KCs also recruited platelet help in response to other strains of bacteria (for example, MRSA). It is also tempting to speculate that these data hint at the possibility of platelet immunity being required for *B. anthracis* and other deadly bacterial strains. Indeed, *B anthracis* is a closely related strain of *B. cereus*, and also directly damages endothelial cells by pathogenic factors *in vitro*[38], not dissimilar to what we observed *in vivo* with *B. cereus*. *B. cereus* isolates have also been implicated in lethal infections from both food and blood contamination with similar clinical presentation to *B. anthracis*. Despite the presence and accumulation of immune cells at the site of *Bacillus* infection, these infections are characterized by bacteremia and severe tissue damage leading to death[12]. In fact, *B. cereus* contains many bacterial factors that induce phagocytic cell death[13–15], and potentially cause major host tissue damage, compromising the antimicrobial immune response. Intriguingly, recent work has shown that members of the *Bacillus* family can induce platelet aggregation within minutes following the exposure of *B. cereus* to human or mouse blood in an *in vitro* flow chamber assay[26]. Our data suggest that this aggregation serves to enlist the help of platelets to encase and restrict the escape of bacteria from KCs.

Although the spleen is often thought to be a key site of bacterial capture[39, 40], the liver is the major site of bacterial trapping for *B. cereus* (this study) and numerous other pathogens[41]. A ten- to hundred-fold greater accumulation of *B. cereus* and *S. aureus* (data not shown) was seen in liver than spleen and imaging revealed much of this capture occurred via the KC. Bacterial capture alone was not sufficient to eradicate these two specific pathogens, and in

fact, it was necessary for KCs to recruit platelets via GPIb. Using flow cytometry, platelet GPIb has recently been reported to bind bacteria directly, transporting bacteria to macrophages[35]. However, directly tracking the KCs, platelets and bacteria *in vivo*, we found that the platelet used GPIb to tether to and then via GPIIb firmly adhere to the vWF constitutively expressed on the surface of KCs. This tethering and binding of platelets to KC serves to co-localize the bacteria with the platelets and increases the chances that platelets find bacteria in blood.

Importantly our data demonstrate that platelets arrive at sites of infection in liver much faster than neutrophils. Furthermore, as they outnumber all other leukocytes in the vasculature tenfold, thus platelets could be of great benefit in some vascular infections. In fact, in the absence of platelets, or the absence of GPIb (resulting in platelets being unable to localize to sites of infection) we observed rapid death of both the KCs and endothelium, increased leakage of plasma out of the vasculature, and host mortality. Platelets can release many anti-microbial molecules and can participate directly in the defense against infection. Platelets have been shown attach to the surface of infected red blood cells and kill malaria parasites directly[34] Furthermore platelets are also capable of stimulating macrophage to improve their killing function. Indeed, the platelet is responsible for more than 95% of the circulating CD40L, an important activator of macrophages, enhancing their ability to kill ingested microbes[42]. Interestingly, in the absence of platelets, the KCs were less effective at catching foreign particles, suggesting that platelets either improve Kupffer cell function or more likely prevent the demise of KC function. Given the critical role platelets play in the ability of the host to capture and clear certain bacteria, it is intriguing to speculate that the recent observed increase in community acquired MRSA infections and the increased usage of aspirin, a potent platelet activation inhibitor, may in some way be related.

Clearly, platelets have more intricate and diverse roles in immune responses than have been previously recognized. Our data reveal an important role for rapid platelet aggregation and encasement of MRSA and *B. cereus* preventing bacteremia and pathogen-induced endothelial permeability, liver dysfunction and mortality. The ongoing surveillance behavior of platelets leads to a near-instantaneous recruitment of platelets (within seconds) to the KC surface and is critical to the host response following *B. cereus* and MRSA infection. Importantly, this platelet recruitment occurs long before classic innate immune effector cells (neutrophils) are recruited. Our data reveal a previously unrecognized, and essential sentinel program for platelets in certain bacterial infection.

METHODS AND MATERIALS

Mice

All protocols used were in accordance with the guidelines drafted by the University of Calgary Animal Care Committee and the Canadian Council on the Use of Laboratory Animals. Wild-type and *C3*$^{-/-}$ mice on the C57BL/6 background mice were purchased from Jackson Laboratory. *GpIbα*$^{-/-}$ mice on the C57BL/6 background were a gift from T. Chavakis (Dresden University of Technology, Dresden, Germany). *Cd41-yfp*$^{ki/ki}$ mice were a gift from K. McNagny (University of British Columbia, Vancouver, BC, Canada). Mice

were maintained in a specific pathogen-free, double-barrier unit at the University of Calgary. Mice of 8–12 weeks old with a weight of 20–24 g were used in the study.

Antibodies and Treatments

For intravital imaging, Phycoerythrin (PE)-conjugated Armenian hamster anti-mouse CD49b (clone HMα2; 3.5 μg/mouse) was purchased from BD Biosciences Pharmingen. Alexa Fluor 647-conjugated rat anti-mouse F4/80 (clone BM8; 2.5 μg/mouse) was purchased from eBioscience. Unconjugated rat anti-mouse PECAM-1 (clone 390) antibodies were purchased from eBioscience and conjugated to Alexa Fluor 647 using a protein labeling kit as per the manufacturer's instructions (Invitrogen). Necrotic cells were visualized by intravenous administration of 5 μl 2.5 mM propidium iodide (PI, Sigma).

Platelet depletion was performed by i.p. injection of 100 μl of anti-thrombocyte serum (Cedarlane) 24 h prior to infection. To inhibit von Willebrand Factor (vWF), each mouse was injected with 50 μg polyclonal rabbit anti-human vWF antibody (DAKO) 30 min prior to infection intravenously. Normal rabbit serum was administered as control in the same way. Kupffer cell depletion was achieved by i.v. injection of 200 μl of clodronate liposomes (CLL; www.ClodronateLiposomes.org; [43, 44] 30 h prior to infection. To assess the trapping capabilities of Kupffer cells *in vivo*, inert fluorescent polychromatic microspheres (Polysciences, Inc.) were administered at 5×10^7 intravenously.

Bacteria

The *B. cereus* strain used in this study was green-fluorescent-protein (GFP) expressing *B. cereus* UW85 43–25[45], kindly provided by R. R. Pompano (University of Chicago) along with R. F. Ismagilov (California Institute of Technology, Pasadena, CA)[26]. For each experiment, *B. cereus* was freshly inoculated from glycerol stocks (15%) into 5 ml Luria Bertani (LB) medium containing 20 μg/ml chloramphenicol (EMD Chemicals). *B. cereus* was grown for 16 h on a rotary shaker at 37 °C. The culture was then diluted 1:10 in fresh LB medium containing 20 μg/ml chloramphenicol and grown for another 2 h until the density reached approximately 1×10^8 colony forming units (CFU)/ml (measured via optical density at 660 nm). Mice were infected with 5×10^7 CFU *B. cereus* intravenously. For experiments with heat-killed *B. cereus*, 5×10^7 CFU/ml *B. cereus* in LB medium were heat killed for 30 min at 99 °C. The heat-killed bacteria were washed with saline and resuspended for injection into mice. For intraperitoneal infection studies, mice were infected with 2×10^7 CFU *B. cereus*.

The Methicillin-susceptible *S. aureus* (MSSA; Xen29) strain used in this study was the 12600 strain, also designated as NCTC8532. Log-phase growth was achieved after 2 h post-subculture in 5 ml LB medium containing 200 μg/ml kanamycin (EMD Chemicals). The Methicillin-resistant *S. aureus* (MRSA) strain used in this study was the USA300 strain. Log-phase growth was achieved after 1.5 h post-subculture in 5 ml BHI medium containing 100 μg/ml chloramphenicol (EMD Chemicals). Mice were infected with 5×10^7CFU labeled with 2.5 μM Syto9 dye of either strain of *S. aureus* intravenously.

Intravital spinning disk confocal microscopy of the liver

For all experiments, mice were anesthetized by intra-peritoneal (i.p.) injection of 200 mg/kg ketamine (Bayer Inc Animal Health) and 10 mg/kg xylazine (Bimeda-MTC). Murine liver intravital microscopy was performed as previously described[46]. Briefly, the tail vein of the anesthetized mice was cannulated to administer fluorescently labeled antibodies and/or additional anesthetic as required. Body temperature was maintained at 37 °C using an infrared heat lamp. Mice were placed in a right lateral position on an adjustable microscope stage. A lateral abdominal incision along the costal margin to the midaxillary line was made to exteriorize the liver, and all exposed tissues were moistened with saline-soaked gauze to prevent dehydration.

The liver was prepared for *in vivo* microscopic observation. Briefly, the liver was placed on the pedestal of an inverted microscope and the liver surface was then covered with a small piece of saline-soaked KimWipe to hold the organ in position. The liver microvasculature was visualized using a spinning-disk confocal microscopy and images were acquired with an Olympus IX81 inverted microscope (Olympus), equipped with an Olympus focus drive and a motorized stage (Applied Scientific Instrumentation). This microscope is fitted with a motorized objective turret equipped with UPLANSAPO 10x/0.40 and UPLANSAPO 20x/0.70 objective lenses and is mounted to an optical table to minimize vibration when imaging. The microscope was equipped with a confocal light path (WaveFx, Quorum) based on a modified Yokogawa CSU-10 head (Yokogawa Electric Corporation).

Three laser excitation wavelengths (491-, 561-, and 642-nm; Cobolt) were used in rapid succession and fluorescence was visualized through one of ET 525/50M (green channel), FF 593/40 (red channel), or ET 700/75M (far red channel) band pass emission filters (Semrock). A 512×512 pixel back-thinned electron-multiplying charge-coupled device camera (C9100-13, Hamamatsu) was used for fluorescence detection. Volocity Acquisition software (Improvision) was used to drive the confocal microscope. Auto contrast was used. Typical laser power, exposure time and sensitivity settings are as follows; green channel (autofluorescence) 74%, 300 ms, 228; red channel 91%, 150 ms, 211; far red channel 81%, 300 ms, 205. Green, red, and far red channels were overlaid using brightest point settings before exporting in .tiff or .avi format.

Intravital spinning disk confocal microscopy of the brain, muscle and ear

A detailed description of the microscopy settings for these tissues has been described elsewhere[27]. Surgical preparation for intravital microscopy for each tissue is briefly described below.

For brain microscopy, the animal’s head was held in a stereotaxic board to isolate movement. Skin covering the parietal bone of the mouse skull was reflected and the left parietal bone was carefully thinned using a high-speed drill (Fine Science Tools) to allow for transillumination. Care was taken as to not open the cranial vault to ensure physiological pressures and blood flow were maintained. Intravital visualization of leukocyte biology within the pial microvasculature was performed through this thinned skull tissue using an upright microscope.

The mouse cremaster muscle was used to study neutrophil recruitment as previously described. In brief, the anesthetized mouse was placed on a special cremaster preparation board and body temperature was maintained through a heat pad. An incision was made in the scrotal skin to expose the left cremaster muscle, which was then carefully dissected free of the associated fascia. The cremaster muscle was cut longitudinally with a cautery. The testicle and the epididymis were separated from the underlying muscle and were moved into the abdominal cavity. The muscle was held flat on an optically clear viewing pedestal and was secured along the edges with 4–0 suture. The exposed tissue was superfused with 37 °C warmed bicarbonate-buffered saline, pH 7.4 and covered with a coverslip. Intravital visualization of intravascular biology was performed using an upright microscope.

For ear microscopy, the anesthetized mouse was placed on a heat pad to maintain the body temperature and the dorsal hair from the right ear was gently removed using depilatory cream (Nair; Church & Dwight Co., Inc.) without causing any irritation. The ear was carefully flattened out on an elevated preparation board, superfused with 37 °C warmed bicarbonate-buffered saline, pH 7.4, and held in place with a coverslip applied on the dorsal side of the ear. Intravital visualization of intravascular biology was performed using an upright microscope.

Semi-quantitative Analysis of Platelet Aggregates

Snapshots were generated from intravital videos and the images corresponding to the red fluorescence channel alone (PE-conjugated anti-CD49b-labeled platelets) were exported as .tif documents. For analysis of aggregate size and number, images were opened with the ImageJ software package V1.45 (NIH at http://rsb.info.nih.gov/ij/) and image contrast was set to maximum to sharply define the borders of each platelet aggregate. To account for variability in background fluorescence between experiments and between antibody lot, and to eliminate fluorescence attributed to rapidly circulating platelets, the minimum brightness threshold was adjusted for each experiment. This threshold was then applied to images from all treatment groups within the experiment, thereby allowing for direct comparison of aggregate sizes and number between treatment groups. Once the minimum brightness threshold was set for each image, the number of platelet aggregates of 25 or 50 μm^2 per field of view (FOV) was counted using the Analyze Particles function within ImageJ.

Semi-quantitative Analysis of vWF Deposition

Snapshots were generated from intravital videos and the images corresponding to the red fluorescence channel alone (PE-conjugated anti-rabbit vWF or IgG) were exported as .tif documents. For analysis of vWF staining, images were opened with the ImageJ software package V1.45 (NIH at http://rsb.info.nih.gov/ij/) and image contrast was set to maximum to sharply define the borders of staining. Once the minimum brightness threshold was set for each image, the vWF staining per FOV was counted using the Analyze Particles function within ImageJ.

Semi-quantitative Analysis of Necrotic Cells

Necrotic cells were visualized by intravenous administration of 5 μl 2.5 mM propidium iodide (PI, Sigma). The PI was allowed to circulate for 2 min and snapshots of at least three

fields of view per animal were taken between 2 to 5 min of PI administration. Snapshots were exported as .tif documents. For analysis of necrotic cell staining, images were opened with the ImageJ software package V1.45 (NIH at http://rsb.info.nih.gov/ij/) and image contrast was set to maximum to sharply define the borders of staining. Once the minimum brightness threshold was set for each image, the PI-positive necrotic cell staining per FOV was counted using the Analyze Particles function within ImageJ.

Bacteriological Analysis

The anaesthetized mice were washed with 70% ethanol under sterile conditions. Blood was collected by cardiac puncture. The lungs, liver and spleen were removed after thoracotomy, weighed and homogenized. For determination of colony forming units (CFU), 10 μl of tissue homogenate or blood was serially diluted, plated onto LB agar plates supplemented with 20μg/ml chloramphenicol, incubated at 37 °C for 18 h, and bacterial colonies were counted.

Liver injury assessment

The anaesthetized mice were washed with 70% ethanol under sterile conditions. Blood was collected by cardiac puncture in a heparinized syringe. The sample was then centrifuge at 400x*g* for 10 min for the retrieval of plasma. The plasma samples were analyzed for alanine transaminase (ALT) levels as per manufacturer protocol (Biotron Diagnotics Inc.).

Statistical analyses

All values were expressed as mean ± standard error of the mean (SEM). Data were compared either by unpaired two-tailed Student's *t*-test or one-way ANOVA with Bonferroni multiple comparisons post hoc test. Statistical significance was accepted at $P < 0.05$.

Supplementary Material

Refer to Web version on PubMed Central for supplementary material.

Acknowledgments

We thank T. Chavakis (Dresden University of Technology, Dresden, Germany) for *GpIbα*$^{-/-}$ mice; K. McNagny (University of British Columbia, Vancouver, BC, Canada) for *Cd41-yfp*$^{ki/ki}$ mice. We thank J. Handelsman (Yale University, New Haven, CT) for making *B. cereus* GFP strain and R. R. Pompano (University of Chicago) along with R. F. Ismagilov (California Institute of Technology, Pasadena, CA) for providing the *B. cereus* GFP strain. We also thank The Live Cell Imaging Facility funded by the Canadian Foundation for Innovation and P. Colarusso for training and assistance related to microscopy. The work is supported by the Alberta Innovates Health Solutions (C.H.Y.W., C.N.J. and P.K.), the Canadian Institutes of Health Research (P.K.) and the Canada Research Chairs Program (P.K.).

References

1. Crispe IN. The liver as a lymphoid organ. Annu Rev Immunol. 2009; 27:147–163. [PubMed: 19302037]
2. Katz S, Jimenez MA, Lehmkuhler WE, Grosfeld JL. Liver bacterial clearance following hepatic artery ligation and portacaval shunt. J Surg Res. 1991; 51:267–270. [PubMed: 1881140]
3. Rabinovitch M. Professional and non-professional phagocytes: an introduction. Trends Cell Biol. 1995; 5:85–87. [PubMed: 14732160]

4. Kobayashi SD, et al. Rapid neutrophil destruction following phagocytosis of Staphylococcus aureus. J Innate Immun. 2010; 2:560–575. [PubMed: 20587998]
5. Pang YY, et al. agr-Dependent interactions of Staphylococcus aureus USA300 with human polymorphonuclear neutrophils. J Innate Immun. 2010; 2:546–559. [PubMed: 20829608]
6. Dixon TC, Fadl AA, Koehler TM, Swanson JA, Hanna PC. Early Bacillus anthracis-macrophage interactions: intracellular survival survival and escape. Cell Microbiol. 2000; 2:453–463. [PubMed: 11207600]
7. Guidi-Rontani C, Levy M, Ohayon H, Mock M. Fate of germinated Bacillus anthracis spores in primary murine macrophages. Mol Microbiol. 2001; 42:931–938. [PubMed: 11737637]
8. Guidi-Rontani C, Weber-Levy M, Labruyere E, Mock M. Germination of Bacillus anthracis spores within alveolar macrophages. Mol Microbiol. 1999; 31:9–17. [PubMed: 9987105]
9. Ramarao N, Lereclus D. The InhA1 metalloprotease allows spores of the B. cereus group to escape macrophages. Cell Microbiol. 2005; 7:1357–1364. [PubMed: 16098222]
10. Mock M, Fouet A. Anthrax. Annu Rev Microbiol. 2001; 55:647–671. [PubMed: 11544370]
11. Hoffmaster AR, et al. Identification of anthrax toxin genes in a Bacillus cereus associated with an illness resembling inhalation anthrax. Proc Natl Acad Sci USA. 2004; 101:8449–8454. [PubMed: 15155910]
12. Miller JM, et al. Fulminating bacteremia and pneumonia due to Bacillus cereus. J Clin Microbiol. 1997; 35:504–507. [PubMed: 9003628]
13. Alfaro DV 3rd, et al. Experimental posttraumatic Bacillus cereus endophthalmitis in a swine model. Efficacy of intravitreal ciprofloxacin, vancomycin, and imipenem. Retina. 1996; 16:317–323. [PubMed: 8865392]
14. Guillemet E, et al. The InhA metalloproteases of Bacillus cereus contribute concomitantly to virulence. J Bacteriol. 2010; 192:286–294. [PubMed: 19837797]
15. Tran SL, et al. Haemolysin II is a Bacillus cereus virulence factor that induces apoptosis of macrophages. Cell Microbiol. 2011; 13:92–108. [PubMed: 20731668]
16. Semple JW, Italiano JE Jr, Freedman J. Platelets and the immune continuum. Nat Rev Immunol. 2011; 11:264–274. [PubMed: 21436837]
17. Aslam R, et al. Platelet Toll-like receptor expression modulates lipopolysaccharide-induced thrombocytopenia and tumor necrosis factor-alpha production in vivo. Blood. 2006; 107:637–641. [PubMed: 16179373]
18. Clark SR, et al. Platelet TLR4 activates neutrophil extracellular traps to ensnare bacteria in septic blood. Nat Med. 2007; 13:463–469. [PubMed: 17384648]
19. Weyrich AS, et al. Signal-dependent translation of a regulatory protein, Bcl-3, in activated human platelets. Proc Natl Acad Sci USA. 1998; 95:5556–5561. [PubMed: 9576921]
20. Weyrich AS, et al. Dipyridamole selectively inhibits inflammatory gene expression in platelet-monocyte aggregates. Circulation. 2005; 111:633–642. [PubMed: 15668340]
21. McDonald B, Urrutia R, Yipp BG, Jenne CN, Kubes P. Intravascular Neutrophil Extracellular Traps Capture Bacteria from the Bloodstream during Sepsis. Cell host microbe. 2012; 12:324–333. [PubMed: 22980329]
22. Yeaman MR, Bayer AS, Koo SP, Foss W, Sullam PM. Platelet microbicidal proteins and neutrophil defensin disrupt the Staphylococcus aureus cytoplasmic membrane by distinct mechanisms of action. J Clin Invest. 1998; 101:178–187. [PubMed: 9421480]
23. Yeaman MR, Tang YQ, Shen AJ, Bayer AS, Selsted ME. Purification and in vitro activities of rabbit platelet microbicidal proteins. Infect Immun. 1997; 65:1023–1031. [PubMed: 9038312]
24. Cole AM, et al. Cutting edge: IFN-inducible ELR- CXC chemokines display defensin-like antimicrobial activity. J Immunol. 2001; 167:623–627. [PubMed: 11441062]
25. Kerrigan SW, et al. A role for glycoprotein Ib in Streptococcus sanguis-induced platelet aggregation. Blood. 2002; 100:509–516. [PubMed: 12091342]
26. Kastrup CJ, et al. Spatial localization of bacteria controls coagulation of human blood by ‘quorum acting’. Nat Chem Biol. 2008; 4:742–750. [PubMed: 19031531]

27. Jenne CN, Wong CH, Petri B, Kubes P. The use of spinning-disk confocal microscopy for the intravital analysis of platelet dynamics in response to systemic and local inflammation. PLoS One. 2011; 6:e25109. [PubMed: 21949865]
28. Yip J, Shen Y, Berndt MC, Andrews RK. Primary platelet adhesion receptors. IUBMB Life. 2005; 57:103–108. [PubMed: 16036569]
29. Fuchs B, et al. Flow-based measurements of von Willebrand factor (VWF) function: binding to collagen and platelet adhesion under physiological shear rate. Thromb Res. 2010; 125:239–245. [PubMed: 19853893]
30. Muta T, Iwanaga S. The role of hemolymph coagulation in innate immunity. Curr Opin Immunol. 1996; 8:41–47. [PubMed: 8729445]
31. Yeaman MR. Platelets in defense against bacterial pathogens. Cell Mol Life Sci. 2010; 67:525–544. [PubMed: 20013024]
32. Czapiga M, Gao JL, Kirk A, Lekstrom-Himes J. Human platelets exhibit chemotaxis using functional N-formyl peptide receptors. Exp Hematol. 2005; 33:73–84. [PubMed: 15661400]
33. Yeaman MR. The role of platelets in antimicrobial host defense. Clin Infect Dis. 1997; 25:951–968. [PubMed: 9402338]
34. McMorran BJ, et al. Platelets kill intraerythrocytic malarial parasites and mediate survival to infection. Science. 2009; 323:797–800. [PubMed: 19197068]
35. Verschoor A, et al. A platelet-mediated system for shuttling blood-borne bacteria to CD8alpha+ dendritic cells depends on glycoprotein GPIb and complement C3. Nat Immunol. 2011; 12:1194–1201. [PubMed: 22037602]
36. Hoffmeister KM, et al. The clearance mechanism of chilled blood platelets. Cell. 2003; 112:87–97. [PubMed: 12526796]
37. Garcia VV, Coppola R, Mannucci PM. The role of the spleen in regulating the plasma levels of factor VIII--von Willebrand's factor after DDAVP. Blood. 1982; 60:1402–1406. [PubMed: 6814552]
38. Popova TG, Millis B, Bailey C, Popov SG. Platelets, inflammatory cells, von Willebrand factor, syndecan-1, fibrin, fibronectin, and bacteria co-localize in the liver thrombi of Bacillus anthracis-infected mice. Microb Pathog. 2011; 52:1–9. [PubMed: 22001909]
39. Altamura M, et al. Splenectomy and sepsis: the role of the spleen in the immune-mediated bacterial clearance. Immunopharmacol Immunotoxicol. 2001; 23:153–161. [PubMed: 11417844]
40. Wellmer A, et al. Experimental pneumococcal meningitis: impaired clearance of bacteria from the blood due to increased apoptosis in the spleen in Bcl-2-deficient mice. Infect Immun. 2004; 72:3113–3119. [PubMed: 15155612]
41. Lee WY, et al. An intravascular immune response to Borrelia burgdorferi involves Kupffer cells and iNKT cells. Nat Immunol. 2010; 11:295–302. [PubMed: 20228796]
42. Soong L, et al. Disruption of CD40-CD40 ligand interactions results in an enhanced susceptibility to Leishmania amazonensis infection. Immunity. 1996; 4:263–273. [PubMed: 8624816]
43. Van Rooijen N, Sanders A. Kupffer cell depletion by liposome-delivered drugs: comparative activity of intracellular clodronate, propamidine, and ethylenediaminetetraacetic acid. Hepatology. 1996; 23:1239–1243. [PubMed: 8621159]
44. van Rooijen N, Sanders A, van den Berg TK. Apoptosis of macrophages induced by liposome-mediated intracellular delivery of clodronate and propamidine. J Immunol Methods. 1996; 193:93–99. [PubMed: 8690935]
45. Dunn AK, Handelsman J. A vector for promoter trapping in Bacillus cereus. Gene. 1999; 226:297–305. [PubMed: 9931504]
46. Wong CH, Jenne CN, Lee WY, Leger C, Kubes P. Functional innervation of hepatic iNKT cells is immunosuppressive following stroke. Science. 2011; 334:101–105. [PubMed: 21921158]

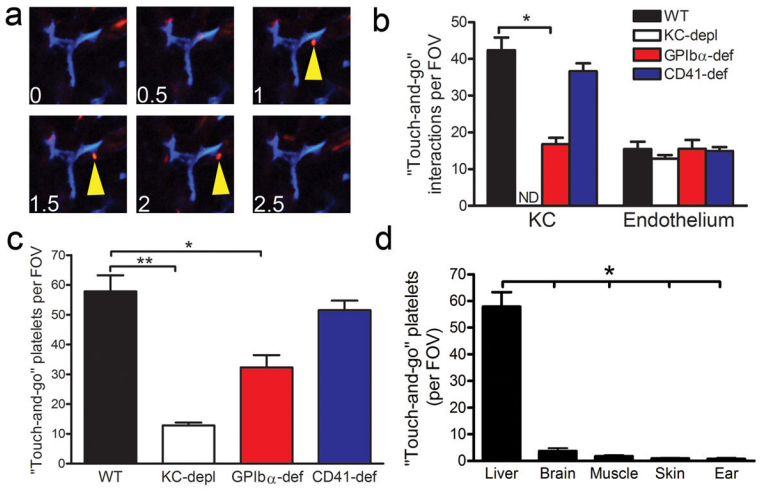

Figure 1. Platelets form "touch-and-go" interactions within the liver sinusoids

(**a**) Representative intravital microscopy images of wild-type mouse liver. Platelets labeled with PE-conjugated anti-CD49b (red); Kupffer cells labeled with Alexa Fluor 647-conjugated anti-F4/80 (blue). Yellow arrows denote rapid and transient "touch-and-go" behavior of platelets on KC. (**b**) Quantification of the number of platelet "touch-and-go" interactions with KC or the endothelium within the livers of wild-type, KC-depleted (KC-depl), *GpIbα*$^{-/-}$ (GPIbα-def) and *Cd41-yfp*$^{ki/ki}$ (CD41-def) mice in basal conditions. $n \geq 3$ individual mice per group; error bars, SEM; $^{*}P < 0.01$ by one-way ANOVA. (**c**) Quantification of the total number of platelet "touch-and-go" interactions within the livers of wild-type, KC-depleted, *GpIbα*$^{-/-}$ (GPIbα-def) and *Cd41-yfp*$^{ki/ki}$ (CD41-def) mice in basal conditions. $n \geq 3$ individual mice per group; error bars, SEM; $^{*}P < 0.01$; $^{**}P < 0.001$ by one-way ANOVA. (**d**) Quantification of the total number of platelet "touch-and-go" interactions within the livers, brain, muscle, skin and ear of wild-type in basal conditions. $n \geq 3$ individual mice per group; error bars, SEM; $^{*}P < 0.001$ vs Liver, one-way ANOVA. See also Supplementary Video 1.

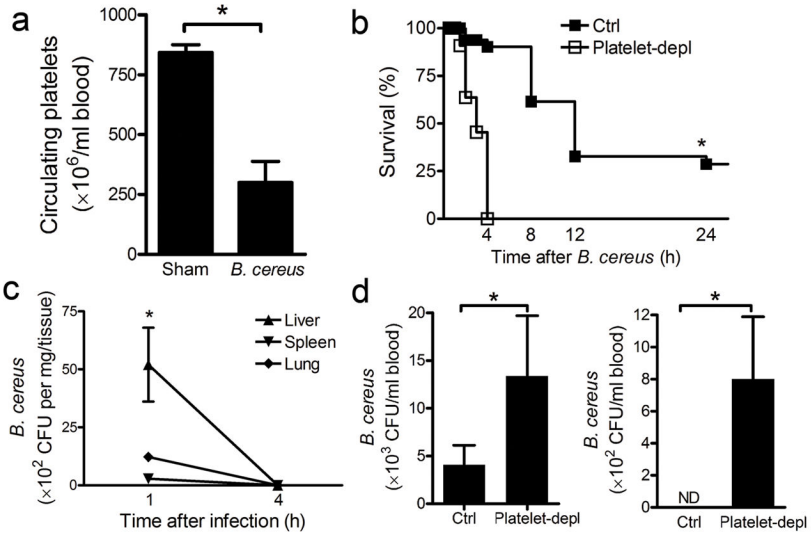

Figure 2. Systemic thrombocytopenia after *B. cereus* infection

(**a**) Circulating platelet counts from sham wild-type mice and mice intravenously infected with 5×10^7 CFU *B. cereus* for 4 h. $n \geq 6$ individual mice per group; error bars, SEM; $^*P < 0.001$ by *t* test. (**b**) Survival rate of *B. cereus*-infected wild-type mice treated with control (Ctrl) or platelet depletion serum (Platelet-depl). $n \geq 10$ per group. $^*P < 0.001$. (**c**) Bacteriological analysis of liver, spleen and lung of wild-type mice at 1 and 4 h after *B. cereus* infection. $n \geq 4$ individual mice per group; error bars, SEM; $^*P < 0.001$, *t* test. (**d**) Bacteriological analysis of peripheral blood of wild-type mice treated with control (Ctrl) or platelet depletion serum (Platelet-depl) at 1 and 4 h after *B. cereus* infection.. $n \geq 10$ per group; error bars, SEM; $^*P < 0.01$, *t* test.

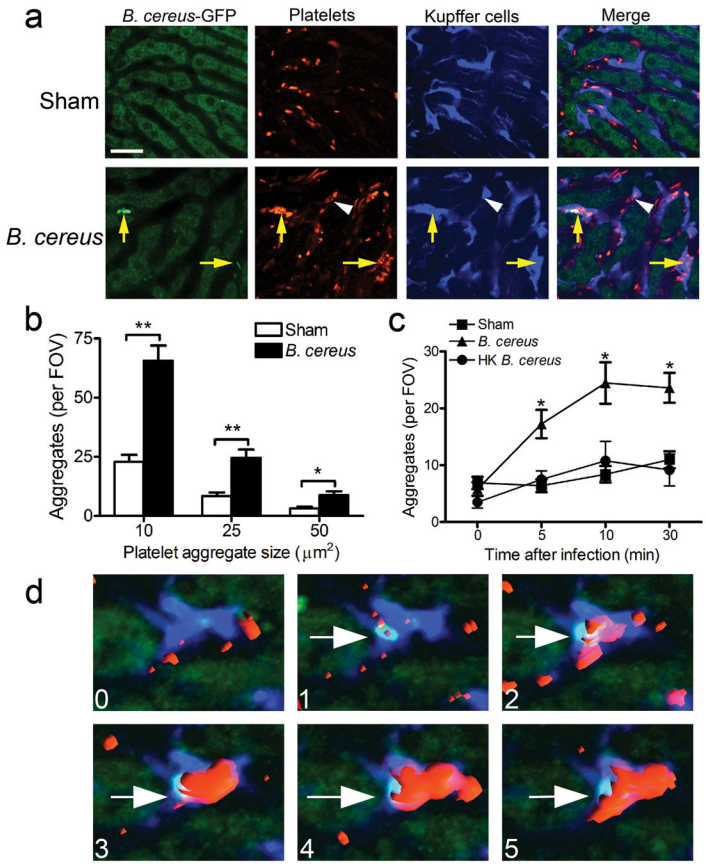

Figure 3. Platelets aggregate after *B. cereus* infection *in vivo*

(**a**) Representative intravital microscopy images of livers from mice intravenously infected with 5×10^7 CFU *B. cereus* for 10 min. Platelets labeled with PE-conjugated anti-CD49b (red); Kupffer cells labeled with Alexa Fluor 647-conjugated anti-F4/80 (blue). Yellow arrows denote colocalization of *B. cereus* and platelet aggregates. White arrowhead denotes platelet aggregation independent of *B. cereus*. Scale bar, 25 μm. (**b**) Quantification of the number of platelet aggregates per field of view (FOV) within liver sinusoids that were larger than 10, 25 and 50 μm^2 following sham or 10 min post *B. cereus* infection. $n \geq 4$ individual mice per group; error bars, SEM; $*P < 0.05$; $**P < 0.01$ by *t* test. (**c**) Quantification of the number of platelet aggregates per FOV within liver sinusoids that were larger than 25 μm^2 following sham, live *B. cereus*, or heat-killed (HK) *B. cereus*. $n \geq 4$ individual mice per group; error bars, SEM; $*P < 0.05$ by one-way ANOVA. (**d**) Representative 3-D sequential images showing KC (blue) captures *B. cereus* (green) and initiates platelet aggregation (red) within liver sinusoids during the first 5 min post infection *in vivo*. The numbers in each panel represents minutes after infection. White arrows denote the captured *B. cereus* by KC within liver sinusoids. See also Supplementary Video 2.

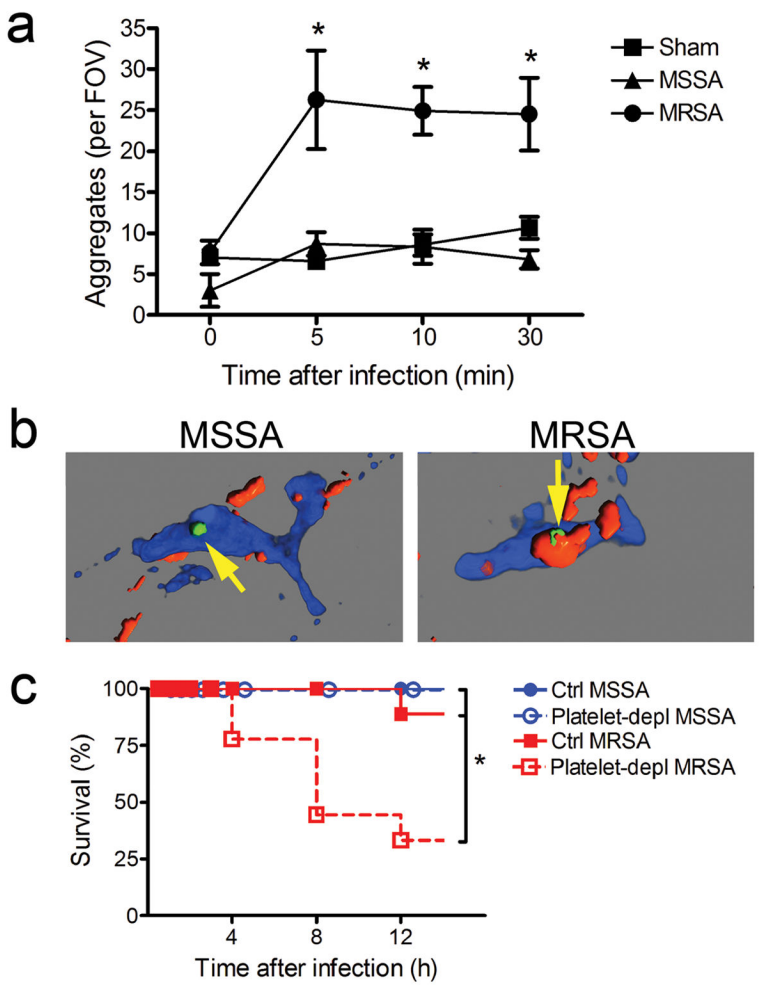

Figure 4. Platelets aggregate after MRSA infection *in vivo*

(**a**) Quantification of the number of platelet aggregates per field of view (FOV) within liver sinusoids that were larger than 25 μm^2 following sham, Methicillin-susceptible *S. aureus* (MSSA; Xen29) or Methicillin-resistant *S. aureus* (MRSA; USA300) infection in wild-type mice. $n \geq 4$ individual mice per group; error bars, SEM; *$P < 0.05$ by one-way ANOVA. (**b**) Representative 3-D reconstructed images showing KC (blue) captures green MSSA (left panel) or MRSA (right panel) and initiates platelet aggregation (red) within liver sinusoids after 10 min of infection *in vivo*. Yellow arrows denote the captured bacteria by KC within liver sinusoids. (**c**) Survival rate of MSSA or MRSA-infected wild-type mice treated with control (Ctrl) or platelet depletion serum (Platelet-depl). $n \geq 9$ per group. *$P < 0.01$.

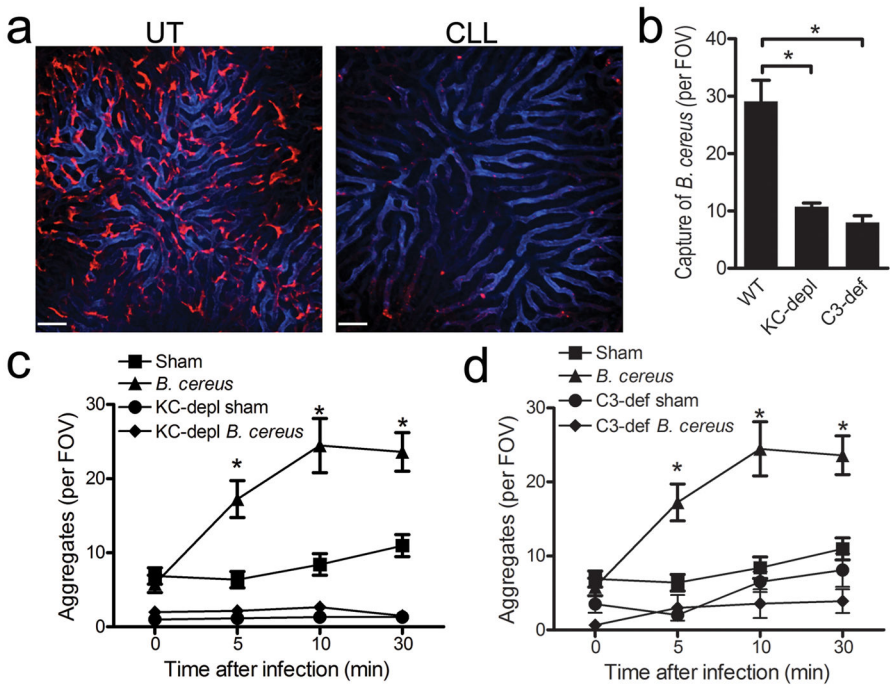

Figure 5. Kupffer cells capture of *B. cereus* is required for platelet aggregation

(**a**) Representative intravital microscopy images of livers from untreated mice (UT) or treated with clondronate liposomes (CLL) to deplete KCs *in vivo*. Kupffer cells labeled with PE-conjugated anti-F4/80 (red) and endothelium labeled with Alexa Fluor 647-conjugated anti-PECAM (blue). Scale bar, 50 μm. (**b**) The number of *B. cereus* bacteria that were captured within liver sinusoids after 10 min of infection were counted in wild-type, KC-depleted (KC-depl) and $C3^{-/-}$ (C3-def) mice. $n \geq 4$ individual mice per group; error bars, SEM; $^{*}P < 0.01$ by one-way ANOVA. (**c**) Quantification of the number of platelet aggregates per FOV within liver sinusoids that were larger than 25 μm^2 following sham or *B. cereus* infection in wild-type and KC-depleted mice. $n \geq 4$ individual mice per group; error bars, SEM; $^{*}P < 0.05$ by one-way ANOVA. (**d**) Quantification of the number of platelet aggregates within liver sinusoids that were larger than 25 μm^2 following sham or *B. cereus* infection in wild-type and $C3^{-/-}$ (C3-def) mice. $n \geq 4$ individual mice per group; error bars, SEM; $^{*}P < 0.05$ by one-way ANOVA. See also Supplementary Video 3.

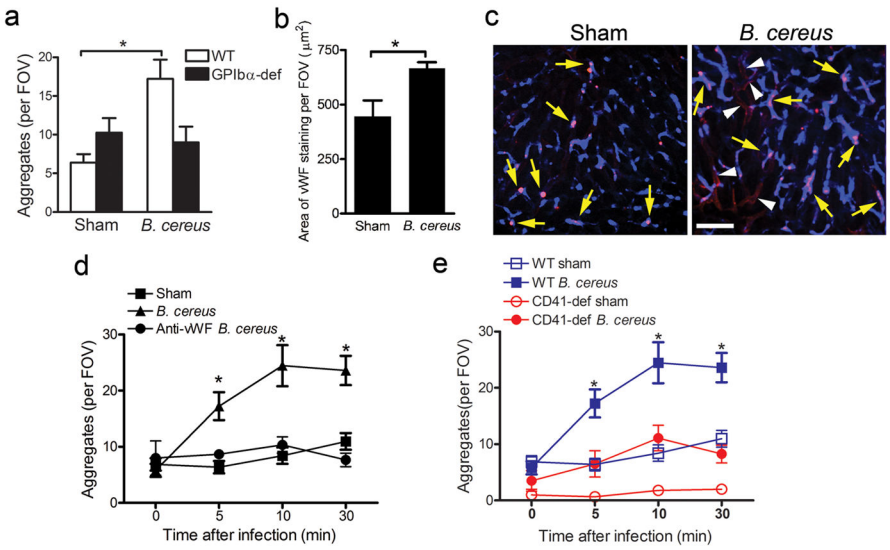

Figure 6. GPIb and GPIIb mediate platelet aggregation after *B. cereus* infection

(**a**) Quantification of the number of platelet aggregates per FOV within liver sinusoids that were larger than 25 μm^2 following sham or following 10 min of *B. cereus* infection in wild-type (WT) and *GpIbα*$^{-/-}$ (GPIbα-def) mice. $n \geq 4$ individual mice per group; error bars, SEM; *$P < 0.05$ by *t* test. (**b**) The area of vWF staining within liver sinusoids was quantified in sham and mice infected with *B. cereus* for 10 min. $n \geq 5$ individual mice per group; error bars, SEM; *$P < 0.05$ by *t* test. (**c**) Representative intravital microscopy images of livers from sham and *B. cereus*-infected mice treated with PE-conjugated anti-rabbit vWF (red) at 10 min. Kupffer cells labeled with Alexa Fluor 647-conjugated anti-F4/80 (blue). Scale bar, 50 μm. (**d**) Quantification of the number of platelet aggregates per FOV within liver sinusoids that were larger than 25 μm^2 following sham or *B. cereus* infection in wild-type and mice that were pretreated with anti-vWF blocking Ab. $n \geq 4$ individual mice per group; error bars, SEM; *$P < 0.05$ by one-way ANOVA. (**e**) Quantification of the number of platelet aggregates per FOV within liver sinusoids that were larger than 25 μm^2 following sham (opened) or *B. cereus* infection (closed) in wild-type (WT; squares) and *Cd41-yfp*$^{ki/ki}$ (CD41-def; circles) mice. $n \geq 4$ individual mice per group; error bars, SEM; *$P < 0.05$ by one-way ANOVA.

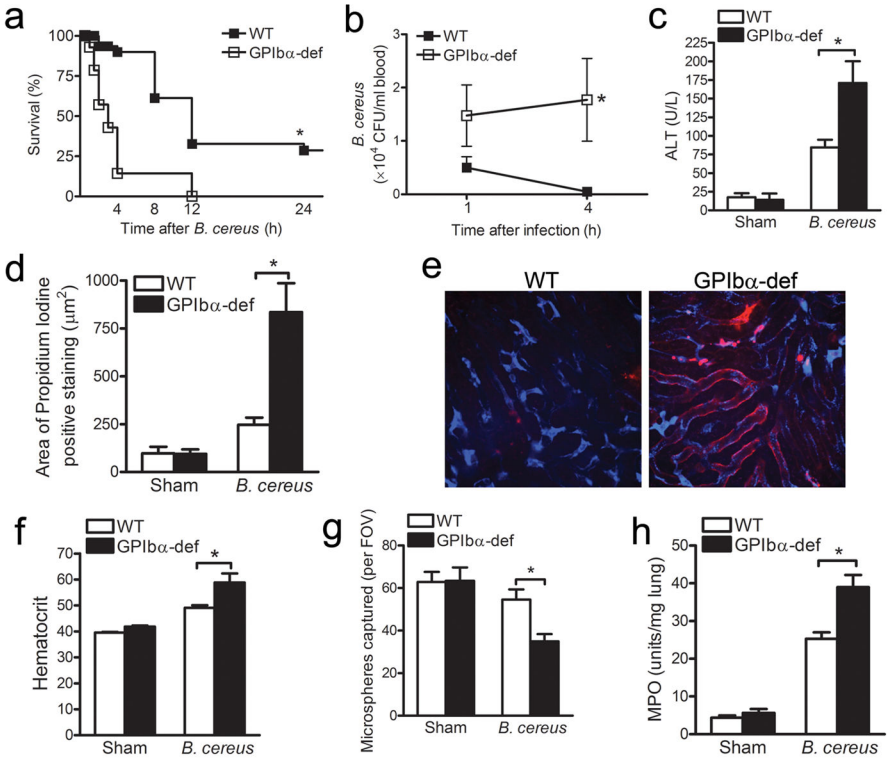

Figure 7. Platelet aggregation following *B. cereus* infection is protective to the host

(**a**) Survival rate of *B. cereus*-infected wild-type (WT) and *GpIbα*$^{-/-}$ (GPIbα-def) mice. $n \geq 10$ per group. *$P < 0.001$. (**b**) Bacteriological analysis of peripheral blood of surviving wild-type (WT) and *GpIbα*$^{-/-}$ (GPIbα-def) mice at 1 and 4 h after *B. cereus* infection. $n \geq 10$ per group; error bars, SEM; *$P < 0.05$ by *t* test. (**c**) Liver damage of sham and *B. cereus*-infected wild-type (WT) and *GpIbα*$^{-/-}$ (GPIbα-def) mice at 4 h was measured via plasma concentrations of alanine transaminase (ALT). $n \geq 6$ individual mice per group; error bars, SEM; *$P < 0.05$ by two-way ANOVA. (**d**) Quantification of the area of propidium iodide-positive staining within the livers of wild-type (WT) and *GpIbα*$^{-/-}$ (GPIbα-def) mice following sham or *B. cereus* infection at 4 h. $n \geq 4$ individual mice per group; error bars, SEM; *$P < 0.01$ by two-way ANOVA. (**e**) Representative intravital microscopy images of livers from wild-type (WT) and *GpIbα*$^{-/-}$(GPIbα-def) mice intravenously infected with 5×10^7 CFU *B. cereus* for 4 h. Necrotic cells labeled with propidium iodide (red); Kupffer cells labeled with Alexa Fluor 647-conjugated anti-F4/80 (blue). Scale bar, 50 μm. (**f**) The hematocrit of the peripheral blood was measured following sham or *B. cereus* infection in wild-type (WT) and *GpIbα*$^{-/-}$ (GPIbα-def) mice at 4 h. $n \geq 6$ individual mice per group; error bars, SEM; *$P < 0.001$ by two-way ANOVA. (**g**) To assess KC function, inert microspheres were administered intravenously after 4 h of *B. cereus* infection. The number of microspheres captured by KCs per FOV after 10 min was counted. $n \geq 4$ individual mice per group; error bars, SEM; *$P < 0.01$ by two-way ANOVA. (**h**) The lungs of sham and *B. cereus*-infected wild-type (WT) and *GpIbα*$^{-/-}$ (GPIbα-def) mice at 4 h were removed and assayed for neutrophil infiltration, as measured by MPO activity. $n \geq 6$ individual mice per group; error bars, SEM; *$P < 0.01$ by two-way ANOVA.